

Ca²⁺ Indicators Based on Computationally Redesigned Calmodulin-Peptide Pairs

Amy E. Palmer,^{1,3} Marta Giacomello,¹
Tanja Kortemme,^{2,4} S. Andrew Hires,¹
Varda Lev-Ram,¹ David Baker,² and Roger Y. Tsien^{1,*}

¹Department of Pharmacology and
Howard Hughes Medical Institute
University of California, San Diego
9500 Gilman Drive
La Jolla, California 92093

²Department of Biochemistry and
Howard Hughes Medical Institute
University of Washington
Seattle, Washington 98195

Summary

The binding interface of calmodulin and a calmodulin binding peptide were reengineered by computationally designing complementary bumps and holes. This redesign led to the development of sensitive and specific pairs of mutant proteins used to sense Ca²⁺ in a second generation of genetically encoded Ca²⁺ indicators (cameleons). These cameleons are no longer perturbed by large excesses of native calmodulin, and they display Ca²⁺ sensitivities tuned over a 100-fold range (0.6–160 μM). Incorporation of circularly permuted Venus in place of Citrine results in a 3- to 5-fold increase in the dynamic range. These redesigned cameleons show significant improvements over previous versions in the ability to monitor Ca²⁺ in the cytoplasm as well as distinct subcellular localizations, such as the plasma membrane of neurons and the mitochondria.

Introduction

Genetically encoded Ca²⁺ sensors have provided a number of advantages over small-molecule fluorescent dyes in studying the dynamics of Ca²⁺ signaling in live cells. Among the desired features are the ability to target indicators to individual subcellular locations, fuse the indicator to a protein of interest to monitor Ca²⁺ in micro- or nanodomains, and generate transgenic organisms for cell-specific targeting and expression within tissues that can not be loaded with fluorescent dyes. Genetically encoded Ca²⁺ indicators can be generally categorized into two classes: (1) constructs such as cameleons in which Ca²⁺-responsive elements alter the efficiency of fluorescence resonance energy transfer (FRET) between two fluorescent proteins [1–5], and (2) probes (camgaros [6, 7], G-CaMP [8], and pericams [9]) in which Ca²⁺-responsive elements, including calmodulin (CaM),

are inserted into a single fluorescent protein to modulate the protonation state of its chromophore. In the original cameleons, the Ca²⁺-responsive elements were comprised of CaM and the CaM binding peptide of skeletal muscle myosin light chain kinase (skMLCK, or M13) and a subsequent design incorporating the peptide from CaM-dependent kinase kinase (CKKp) in place of skMLCK [4]. More recently, Heim and Griesbeck successfully replaced the CaM-skMLCK portion with tropomyosin C from chicken skeletal muscle and human cardiac muscle [5, 10].

To date, these genetically encoded Ca²⁺ indicators have been targeted to the nucleus [1], endoplasmic reticulum (ER) [1, 11], mitochondria [12, 13], Golgi [7], and plasma membrane [5, 10, 14] of individual cells. In addition, indicators have been expressed in a number of transgenic animals [15–20]. However, there are still a number of shortcomings of the genetically encoded indicators. In particular, there are potential problems with indicators binding to and being perturbed by cellular proteins, such as endogenous CaM. An example of this problem is that the cameleons have failed to respond appropriately when targeted to the plasma membrane of neurons ([5] and unpublished data). Because CaM is predicted to be in millimolar concentrations at the mouth of Ca²⁺ channels [21], and because it has been measured to be 0.2–0.4 mM in presynaptic terminals and postsynaptic densities (M. Kennedy and V. Lucic, personal communication), it seemed likely that the failure could be due to binding of endogenous CaM to the peptide portion of the sensor, thus preventing the cameleon from responding to changes in Ca²⁺. Likewise, the cameleons have consistently produced disappointingly small responses in transgenic mice. A recent study by Hasan et al. found, by fluorescence recovery after photobleaching, that a large portion of the cameleon was not freely diffusible; thus, the authors suggested that it might be bound to cellular proteins [22]. Finally, there are still gaps in the Ca²⁺ sensitivity of genetically encoded indicators, particularly at intermediate Ca²⁺ concentrations, making it difficult to find an appropriate sensor to monitor Ca²⁺ in microdomains of moderate to high Ca²⁺. Generating a series of indicators that resist endogenous CaM and have varying Ca²⁺ affinities could prove useful in monitoring Ca²⁺ in distinct subcellular locations as well as in microdomains of high Ca²⁺.

Our goal in redesigning the cameleon was to reengineer the binding interface between CaM and a target peptide to generate selective and specific binding pairs that could not be perturbed by wild-type (wt) CaM. We previously reversed the salt bridge interactions between basic residues in the target peptide and acidic residues in CaM to generate a mutant calmodulin-peptide pair that was unaffected by large concentrations of excess CaM. This redesigned pair led to a Ca²⁺ indicator (D1) with a relatively weak affinity for Ca²⁺ ($K'_d = 60 \mu\text{M}$) and has been used to monitor Ca²⁺ directly in the ER in individual living cells [11]. In the current work, we computationally designed steric bumps in the target peptide and

*Correspondence: rtsien@ucsd.edu

³ Present address: Department of Chemistry and Biochemistry, University of Colorado, Boulder, Colorado 80309.

⁴ Present address: Department of Biopharmaceutical Sciences and California Institute for Quantitative Biomedical Research (QB3), University of California, San Francisco, 1700 4th Street, San Francisco, California 94142.

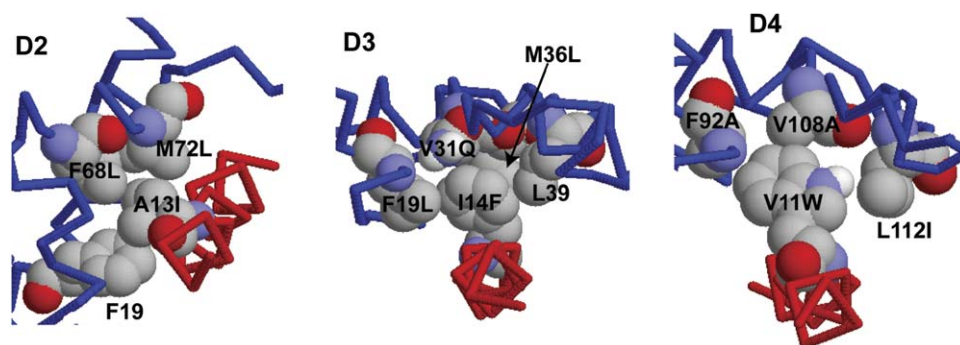


Figure 1. Model Structures of the Computationally Redesigned CaM-Peptide Interface

The backbone of CaM is displayed in blue, and the peptide is shown in red. The mutations for each structure are noted in the figure and are displayed with the space-filled model. Residues F19 (in D2) and L39 (in D3) are noted in the relevant structures, as these residues were allowed to vary in the design phase; however, the final structure retained the wild-type residue.

complementary holes in CaM in order to generate a series of indicators (D2, D3, and D4) with varying Ca^{2+} affinities, including a high-affinity indicator that cannot be perturbed by excess CaM. These indicators show significant improvements in the ability to monitor Ca^{2+} in different subcellular locations such as the plasma membrane of neurons and the mitochondria.

Results and Discussion

Computational Design of Complementary Bumps and Holes

The crystal structure of CaM bound to smooth muscle myosin light chain kinase (smMLCK) [23] was used as the starting point for generating mutant CaM-peptide pairs with altered steric interactions at the interface. A computational Ala scan [24] was performed in order to identify hot spots that contribute significantly to the binding energy of CaM and smMLCK. A hot spot was defined as a residue whose replacement by Ala resulted in a change in the binding energy ($\Delta\Delta G_{\text{bind}}$) of ≥ 1 kcal/mol. The hot spots within the smMLCK peptide are presented in Table S1 (see Supplemental Data available with this article online). Because the peptide forms an α helix around which CaM wraps, we reasoned that to generate a peptide with decreased affinity for wt CaM, we should replace small, but important (as determined by the computational Ala scan), residues with bulkier residues, generating bumps in the peptide that would sterically clash with wt CaM. For this reason, Val11 and Ile14 were targeted. In addition, Ala13, which could not show up in an Ala scan, was chosen because examination of the interactions in the binding interface suggested that this residue made a number of close contacts with CaM, and that replacement with a larger residue could significantly perturb CaM binding.

Two rounds of calculations were performed. In the first round, the designated peptide residue (A13, I14, or V11) was fixed to one of a number of bulky or charged residues, and the interacting and nearby (within 5 Å) residues in CaM were allowed to change conformation (“repacked”) around the mutated peptide residue. The $\Delta\Delta G$ of this repacked pair ($\Delta\Delta G_{\text{repack}}$) was then compared to the $\Delta\Delta G$ of the wt CaM-wt peptide pair to determine whether binding of wt CaM to the mutant peptide would

be destabilized compared to binding the wt peptide. In the second round of calculations, again the mutated peptide residue was fixed, but this time the neighboring residues in CaM were designed (i.e., both sequence and conformational space were sampled) and the lowest-energy structures were selected. This protocol is similar to the “computational second site suppressor” strategy to design protein pairs with altered interaction specificity [25]. In Design 2, involving A13 on the peptide, the following residues in CaM were varied: F19, F68, M72, and M71. For Design 3 (involving I14), F19, M36, L39, and V35 were varied, while, in Design 4 (involving V11), F92, V104, L112, A88, and V91 were varied. The $\Delta\Delta G$ of the designed pair ($\Delta\Delta G_{\text{design}}$) was computed in order to provide an estimate of the strength of the interaction between the mutant peptide and mutant CaM.

The $\Delta\Delta G_{\text{repack}}$ and $\Delta\Delta G_{\text{design}}$ values of the different computationally designed CaM-peptide pairs are presented in Table S2. We selected for further consideration designs with predicted binding affinities ($\Delta\Delta G_{\text{design}}$) equal to or better than that of the wt CaM-wt peptide pair, and for which the designed peptide was predicted to bind only very weakly to wt CaM ($\Delta\Delta G_{\text{repack}}$). With these criteria, the designs involving A13I (Design 2, D2), I14F (Design 3, D3), and V11W (Design 4, D4) were selected. Figure 1 shows model structures highlighting the mutated peptide and CaM residues of D2, D3, and D4.

In Vitro Characterization of the New Cameleons

The mutant CaMs and peptides were cloned between CFP and citrine fluorescent protein [7] or between CFP and circularly permuted Venus (cpV) to yield a new generation of cameleons. Previously, Miyawaki and co-workers showed that incorporation of cpV results in an ~ 5 -fold increase in the ratio change of the YC3 cameleon [14]. Under saturating conditions of Ca^{2+} , all of the cameleons show a decrease in donor emission (CFP) and an increase in acceptor emission (citrine or cpV), indicative of increased FRET caused by Ca^{2+} binding and subsequent conformational change. The representative emission spectra in the presence and absence of 1 mM Ca^{2+} of D3 and D3cpv are presented in Figures 2A and 2B. The spectra of D2 and D4 are similar to that of D3, while the spectra D2cpv and D4cpv are similar to that

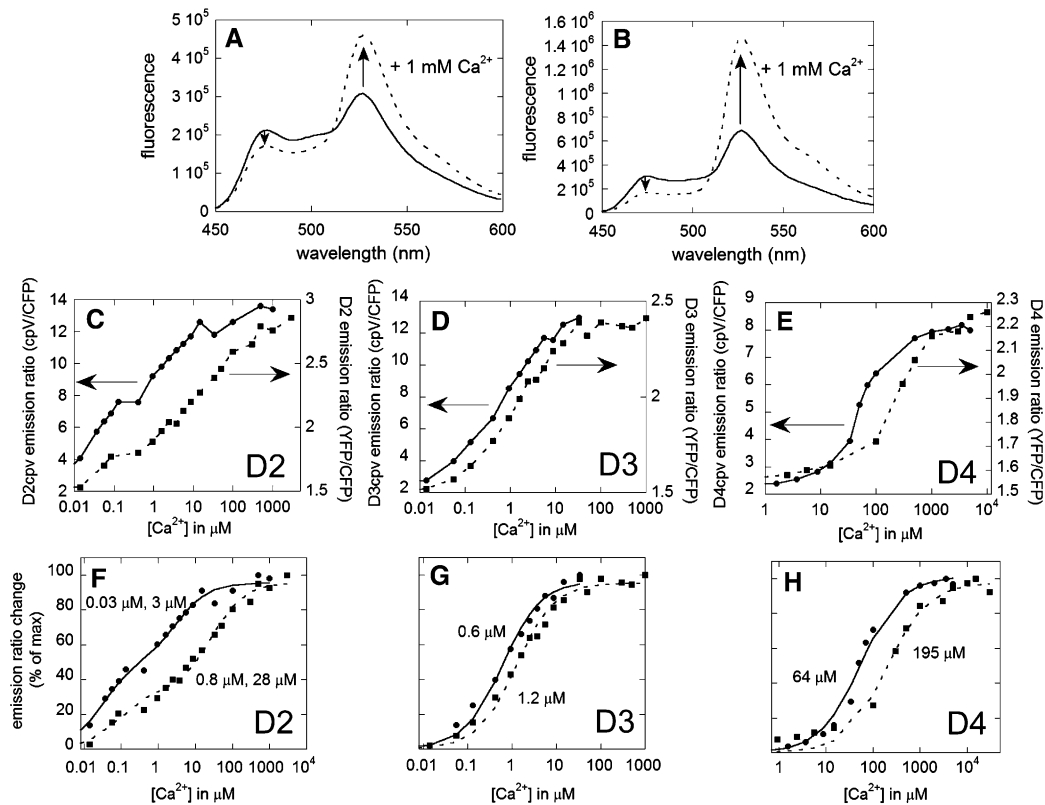


Figure 2. In Vitro Characterization of D2, D3, and D4 along with the cpV Variants

(A) Emission spectrum upon excitation at 420 nm of D3 with (dashed line) and without (solid line) Ca²⁺.
 (B) Emission spectrum upon excitation at 420 nm of D3cpv with (dashed line) and without (solid line) Ca²⁺.
 (C–E) Emission ratio (YFP/CFP) of citrine (squares, dashed line) and cpV (circles, solid line) variants of (C) D2, (D) D3, and (E) D4 as a function of Ca²⁺ concentration. The arrows point to the appropriate y axis scale for cpV and citrine variants.
 (F–H) Ca²⁺ titration curves of citrine and cpV variants of (F) D2, (G) D3, and (H) D4. The data were fit according to the equations described in [Experimental Procedures](#). The K_d values are listed on each plot.

of D3cpv (data not shown). **Figure 2** also presents a comparison of the Ca²⁺ titration curves of the redesigned cameleons with citrine and cpV as the acceptor fluorescent protein. Incorporation of cpV led to an increase in the emission ratio change (5.3 × for D2cpv, 5.1 × for D3cpv, and 3.8 × for D4cpv). **Figure 2** shows the emission ratio (panels C, D, and E) and percent ratio change (panels F, G, and H) as a function of Ca²⁺ concentration for the citrine- and cpV-based sensors. D2 yields a biphasic Ca²⁺ response curve, whereas D3 and D4 can be fit with a single site model. The two dissociation constants of D2 likely result from the different affinities of the N- and C-terminal domains of CaM for Ca²⁺, as observed for YC2.1, YC4.3, and D1 [1, 11].

Figure 3A compares Ca²⁺ titration curves of the redesigned cameleons (D1, D2cpv, D3cpv, and D4cpv) with those of the three previous cameleons (YC2.1, YC3.3, YC4.3) and demonstrates that, by altering the relative affinity for the CaM-peptide pair, the Ca²⁺ sensitivity could be tuned over a wide range. Importantly, the new cameleons fill gaps in Ca²⁺ sensitivity. In particular, D2cpv is sensitive to a wide range of Ca²⁺ concentrations and could be very useful for monitoring Ca²⁺ in microdomains or in the mitochondria, where Ca²⁺ can range from 100 nM up to 100 μM [26]. D3cpv is poised directly between YC2.1 and YC3.3 and would be the most sen-

sitive to modest elevations above basal Ca²⁺ levels. Finally, D4cpv (along with D1) falls between YC3.3 and YC4.3 and could be suitable for imaging higher concentrations of Ca²⁺, such as in microdomains.

An important part of our design strategy was to develop sensors that would not be perturbed by wt CaM. **Figure 3B** shows the FRET response of YC3.3 and the redesigned cameleons in the presence of excess CaM. For YC3.3, the FRET response under saturating Ca²⁺ conditions decreases with the addition of increasing concentrations of CaM. The excess CaM in solution can bind to the peptide portion of the cameleon, forming an intermolecular complex and thus preventing the sensor from undergoing a conformational change and registering a FRET increase in the presence of Ca²⁺. Importantly, two of the three computational designs (D2cpv and D3cpv) show a marked improvement when compared to YC3.3, such that the addition of increasing [CaM] resulted in only a small decrease in the FRET response (<10%), indicating that these cameleons are not perturbed by large excesses of CaM. The FRET response of D4cpv was not as strongly affected as that of YC3.3, but it still showed some perturbation by the addition of excess CaM. In the absence of structural data, it's not clear why this design was not as successful as D2 and D3, but, given the conformational flexibility of

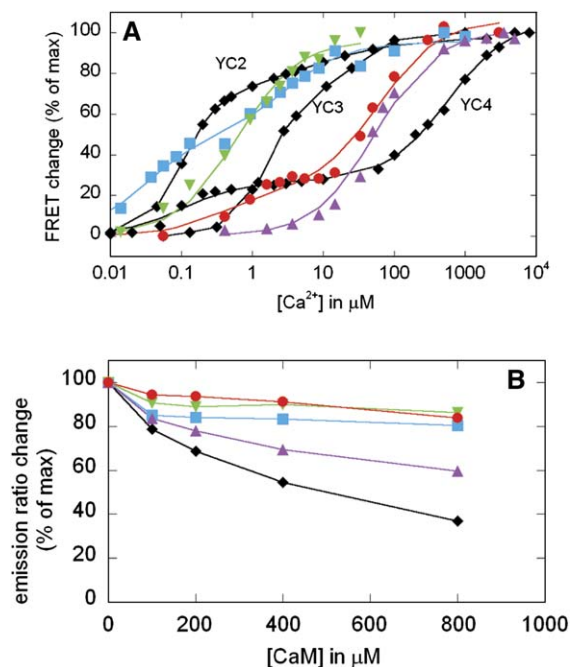


Figure 3. In Vitro Characterization of the Redesigned Cameleons (A) Ca^{2+} titration curves of original and redesigned cameleons. (B) Titration with varying concentrations of wild-type CaM. The original cameleons (YC2, YC3, and YC4; black diamonds) are labeled on the graph. The first redesign, D1, is presented as red circles, and the computational designs are presented as follows: D2cpv, blue squares; D3cpv, green, upside-down triangles; D4cpv, purple triangles.

CaM, it's possible that CaM adopted a conformation other than that in the crystal structure.

The insensitivity of the designed sensors D2 and D3 to even high concentrations of wt CaM (Figure 3B) suggests a significant switch in CaM-peptide specificity of cognate designed pairs over noncognate pairs (wt CaM-mutant peptide complexes). While the measured changes in FRET as a result of Ca^{2+} -dependent confor-

mational changes do not directly monitor differential CaM-peptide binding affinities, the altered D2 and D3 cameleon peptides are not affected in their ability to bind to their cognate mutant CaM even by approximate millimolar concentrations of competing wt CaM. It should be noted that the designed pairs are interacting in *cis* (as part of the cameleon construct), whereas wt CaM is added in *trans*. Moreover, the designed sensors D2, D3, and D4 display a wide range of Ca^{2+} affinities that may reflect differences in the strengths of CaM-peptide interactions. Even with these caveats, there are still few examples of successful computational designs substantially altering protein-protein interaction specificity [25, 27–30]. Shifman and Mayo showed a 155-fold increase in binding specificity for wt CaM binding the smMLCK ligand over other CaM target peptides. In this case, specificity was achieved by explicitly optimizing the binding interface for one ligand. Our complementary approach incorporates aspects of negative design [25, 30] to more dramatically destabilize unwanted interactions and create large specificity switches, although likely at the expense of binding affinity.

Cellular Responses of the New Cameleons: Cytosol and Membrane Targeting

Because D2cpv and D3cpv appear to be the most promising for measuring general Ca^{2+} signaling processes, these cameleons were expressed in mammalian cells. Figure 4 shows the response of D2cpv (Figures 4A and 4B) and D3cpv (Figures 4C and 4D) to conditions that resulted in an increase in cellular Ca^{2+} . Upon treatment of HeLa cells with 100 μM histamine, Ca^{2+} oscillations were observed in the cytosol due to inositol 1,4,5-trisphosphate (IP_3)-dependent release of Ca^{2+} from the ER. The total dynamic range of the sensor is comparable to that of YC3.60, a previous version of cameleon that incorporated cpV [14]. It should be noted that the minimum emission ratio (R_{min}) obtained by treating the cells with iomomycin and EGTA is slightly lower than the resting ratio for both D2cpv and D3cpv (D2cpv: $R_{min} = 3.3$ – 3.4 , $R_{resting} = 3.8$ – 4.0 ; D3cpv: $R_{min} = 2.4$, $R_{resting} = 2.6$ – 3.0),

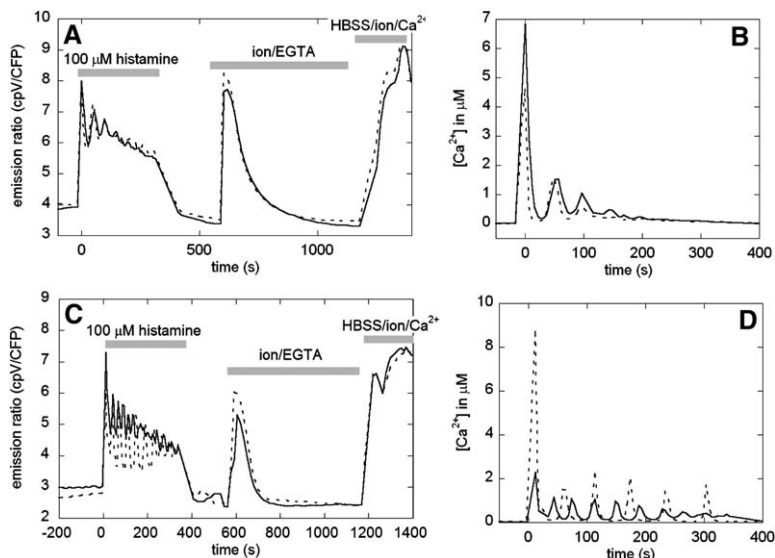


Figure 4. Cellular Responses of the Redesigned Cameleons

(A–D) Response of (A and B) D2cpv and (C and D) D3cpv expressed in the cytosol of HeLa cells to treatments that alter Ca^{2+} . The solid and dashed curves each represent a different cell. In (B) and (D), the emission ratios have been converted to $[Ca^{2+}]$ as described in Experimental Procedures.

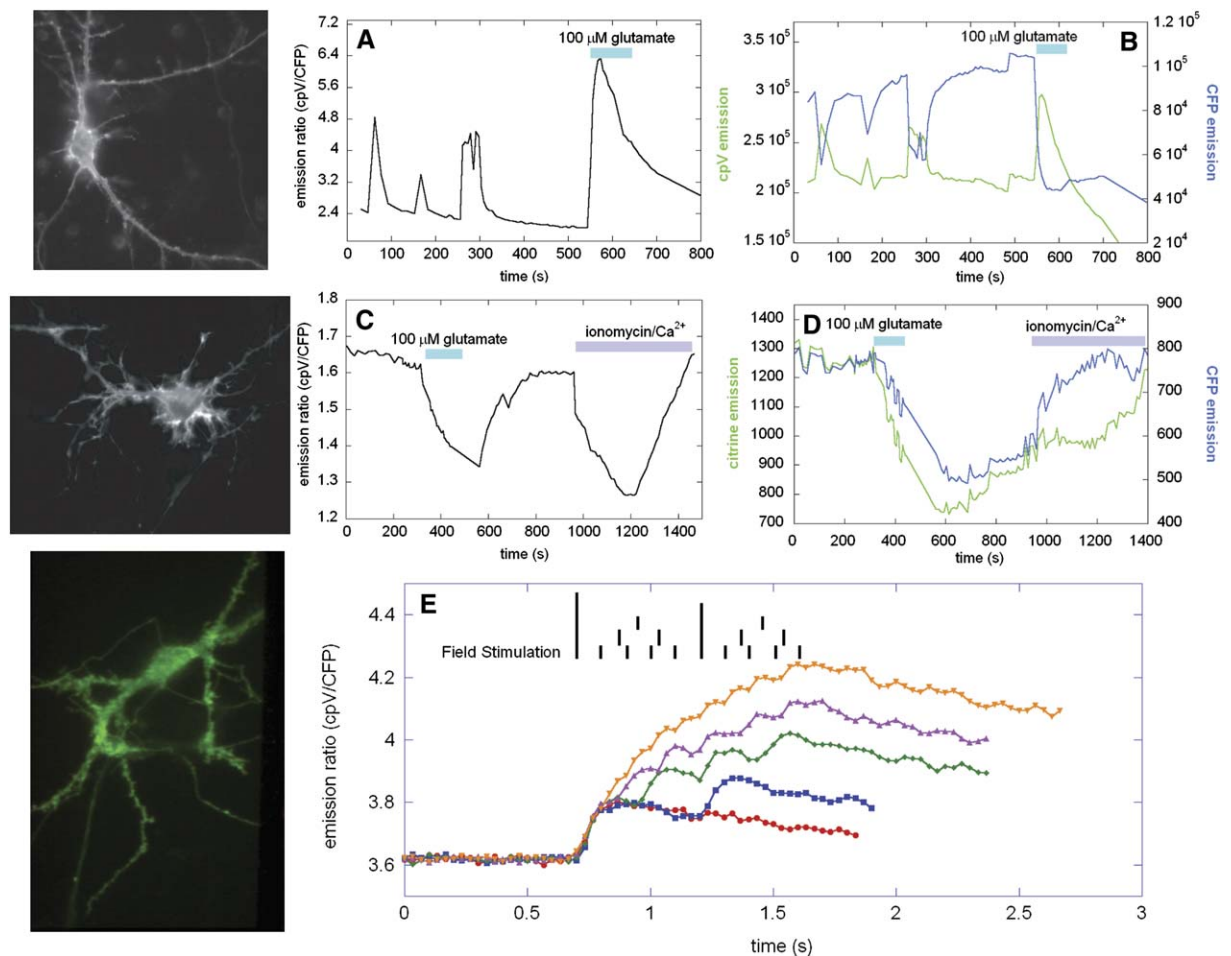


Figure 5. Plasma Membrane-Targeted LynD3cpv and LynYC3.3 in Hippocampal Neurons

Panel on the left-hand side shows an image of neurons expressing the respective constructs.

(A) LynD3cpv upon treatment with 100 μM glutamate (represented by the blue bar). The Ca²⁺ spikes before stimulation represent Ca²⁺ influx from spontaneous activity.

(B) Individual FRET and CFP channels for the experiment presented in (A).

(C) LynYC3.3 upon stimulation with 100 μM glutamate (represented by the blue bar) and treatment with 5 μM ionomycin and 10 mM Ca²⁺ (represented by the gray bar).

(D) Individual FRET and CFP channels for the experiment presented in (C).

(E) Responses of membrane-localized lynD3cpv to field stimulation (1 s) of increasing frequency. Individual stimulations (marked by black lines) are clearly discernable at stimulation rates of up to 10Hz.

indicating that both sensors are ideally poised to monitor changes in resting Ca²⁺ levels. **Figures 4B and 4D** focus in on the changes in Ca²⁺ observed with each sensor; the emission ratio was converted to [Ca²⁺] as described in **Experimental Procedures**. In each experiment, Ca²⁺ in the cytosol increased from $\sim 20\text{--}80$ nM to low micromolar concentrations upon histamine stimulation.

A distinct advantage of genetically encoded sensors over fluorescent dyes is the ability to target specific subcellular locations in order to monitor Ca²⁺ dynamics in well-defined domains within a cell. In particular, membrane-targeted indicators would facilitate investigations of localized processes such as Ca²⁺ influx. However, there have been reports that cameleons do not respond appropriately when targeted to the plasma membrane, particularly in neurons where there are high concentrations of CaM at the mouth of Ca²⁺ channels [5]. In order to test whether our reengineered cameleons remedied this problem, we targeted D3cpv and YC3.3 to the

plasma membrane by attaching a myristoylation-palmitoylation tag to the N terminus, resulting in lynD3cpv and lynYC3.3 [31]. Each construct was expressed in primary rat hippocampal neurons, and the cells were exposed to conditions that led to Ca²⁺ influx (KCl-induced depolarization, exogenous glutamate application, and field stimulation; **Figure 5**). In the neurons expressing lynD3cpv, Ca²⁺ influx due to spontaneous activity could be detected even in the absence of stimulus. Treatment with 100 μM glutamate (**Figure 5A**) resulted in a significant (2- to 3-fold) increase in the FRET response due to Ca²⁺ influx, indicating that the sensor was unencumbered by membrane targeting. The individual fluorescence channels (FRET and direct CFP) are presented in **Figure 5B** and show the expected reciprocal response upon stimulation. When Ca²⁺ was removed from the cytosol by treatment with ionomycin and EGTA, the activity ceased and the ratio dropped just below the starting ratio ($R_{\text{resting}} = 2.0\text{--}2.1$, $R_{\text{min}} = 1.8\text{--}1.9$). In contrast, when

neurons expressing lynYC3.3 were treated with 100 μM glutamate (Figure 5C) or 50 mM KCl (data not shown), the emission ratio decreased slightly and did so with a dramatically delayed time course. We hypothesize that the failure of the lynYC3.3 cameleon was due to interference by endogenous CaM binding to the peptide portion of the sensor, preventing a FRET increase. By creating a mutant CaM-peptide pair orthogonal to wt CaM, we succeeded in assaying $[\text{Ca}^{2+}]$ at the previously inaccessible location of the plasma membrane of neurons. As even the most successful *in vivo* mammalian expression of cameleons has displayed attenuated responses [14], presumably due to continuing endogenous protein interference, we further hypothesize that this reengineered CaM family will show improved response traits in intact organisms.

To probe the limits of lynD3cpv's sensitivity and its suitability for precise studies of neuronal Ca^{2+} signaling, we delivered brief trains of action potentials (APs) with field-stimulating electrodes (Figure 5E). LynD3cpv-transfected cells showed a robust ($\sim 5\%$ – 10% ΔR) Ca^{2+} response to single APs. One-second AP trains were then delivered at increasing frequencies (1–10 Hz). Calcium spikes corresponding to each AP could be unambiguously observed for all frequencies, including 10 Hz, the highest theoretical resolution of our 30 Hz sampling rate.

Our data suggest that in the process of creating FRET-based sensors it may be important to include strategies for preventing interaction of the sensor with endogenous cellular proteins. Incorporation of mutant CaM-peptide pairs into the single fluorescent protein sensors may improve the biological response and versatility of these sensors as well [6–9]. The only protein-based Ca^{2+} sensor that does not rely on CaM is the family of troponin C (TnC)-based cameleon sensors. Although the original TnC sensors suffered from significant Mg^{2+} sensitivity, in elegant protein engineering work, Griesbeck and coworkers succeeded in abolishing this Mg^{2+} sensitivity with only a minor decrease in Ca^{2+} affinity ($K_d = 2.5 \mu\text{M}$) [10]. The authors postulate that this TnC-based sensor, which is also functional at the plasma membrane of neurons, is unlikely to interfere with cellular biochemical pathways because TnC is not as ubiquitous as CaM. This appears to be the case in neurons; however, it remains to be seen whether TnC sensors work in muscle cells, in which TnC is more likely to have endogenous binding partners.

Improvements in Mitochondrial Ca^{2+} Measurements
Mitochondria are critical to many Ca^{2+} signaling processes and have been shown to take up Ca^{2+} from the cytosol as well as to form close connections with the ER [12, 32]. To better understand the origin of different Ca^{2+} signals and the interplay between organelles, we would like to be able to monitor mitochondrial Ca^{2+} directly and quantitatively. Unfortunately, measuring Ca^{2+} in the mitochondria has proven to be challenging. More specifically, the dye Rhod-2 suffers from frequent mislocalization in the cytoplasm, and its intensity-based rather than ratiometric readout is vulnerable to artifacts and difficult to calibrate. Aequorin does not permit single cell measurements or direct visualization of subcellular heterogeneity in mitochondrial Ca^{2+} . Previous cam-

eleons genetically targeted to the mitochondria had low sensitivity and suffered from mislocalization. More recently, Pozzan and coworkers demonstrated that attaching tandem signal sequences from subunit VIII of human cytochrome C oxidase (abbreviated 2mt in their construct) improved specific localization to the mitochondria [13]. However, the localization worsened when they tried to replace the original YFP in the cameleon with improved YFPs (citrine or Venus) that are more resistant to photobleaching and less sensitive to pH [7, 33].

Because D2cpv, D3cpv, and D4cpv displayed a much larger dynamic range than their citrine counterparts, we focused on these versions of the various sensors. Figure 6 shows a comparison between HeLa cells transfected with 2mtYC2 (the previously developed mitochondrially targeted cameleon developed by Pozzan and coworkers) [13], 2mtD2cpv, 2mtD3cpv, and 2mtD4cpv. Treatment of the cells with 100 μM histamine resulted in a rapid rise followed by oscillations in mitochondrial Ca^{2+} . The resting level of Ca^{2+} in the mitochondria was determined to be ~ 50 – 300 nM and was consistent among the three probes with the highest Ca^{2+} affinities. D4cpv tended to report somewhat higher resting levels, but its Ca^{2+} affinity is too weak for these estimates (at very low Ca^{2+} concentrations) to be reliable. Ca^{2+} rises upon histamine treatment were somewhat variable, but Ca^{2+} concentrations in the range of 1.5–200 μM were observed. Interestingly, a large response was still observed with the lowest affinity sensor (2mtD4cpv), indicating that mitochondrial Ca^{2+} levels actually rise substantially and the higher affinity probes are likely to be close to saturation. Figure 6 clearly shows that 2mtD2cpv and 2mtD3cpv exhibit a larger dynamic range and better signal-to-noise ratio than 2mtYC2; thus, they will be much more sensitive to small changes in mitochondrial Ca^{2+} . 2mtD4cpv remains responsive up to higher concentrations of Ca^{2+} and may more accurately report the highest Ca^{2+} concentrations.

We also examined the effect of multiple copies (2mt, 4mt, 6mt, and 8mt) of the CytC signal sequence on localization of our improved cameleons. D2, D2cpv, D3, D3cpv, and D4cpv all expressed well in the mitochondria of HeLa cells, and there were no dramatic differences in localization for the different sensors (i.e., sensors with citrine and cpV exhibited similar localization patterns). In order to compare the localization of sensors with different targeting sequences, the fluorescence intensity of mistargeted fluorescence in the cytosol and nucleus was compared to the average mitochondrial fluorescence in the same cell 48 hr after transfection. A clear improvement was observed by incorporation of multiple repeats of the tandem signal sequence (Figure S1). In addition, we found that the percentage of transfected cells displaying cytoplasmic staining decreased from 35% for 2mt to 20% for 4mt, 5% for 6mt, and 1% for 8mt. However, while the probes with six and eight copies of the CytC signal sequence had the best localization efficiency, the mitochondria were rounded, and a large number of the transfected cells were dying. Therefore, 4mt appeared to be the best construct, as it exhibited a marked improvement in localization without any apparent adverse effects on the mitochondria.

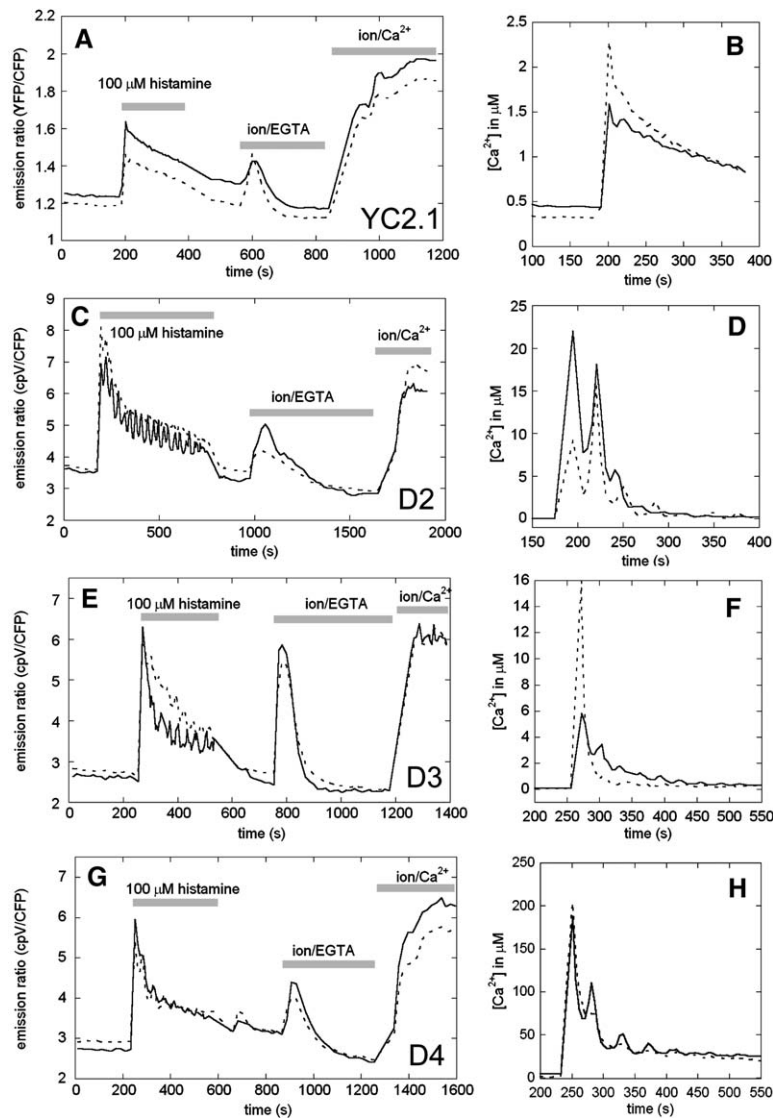


Figure 6. Comparison of Various Mitochondrially Targeted Cameleons

(A–H) (A, C, E, and G) Emission ratio of cells expressing (A) 2mtYC2/pMito, (C) 2mtD2cpv, (E) 2mtD3cpv, or (G) 2mtD4cpv upon treatment with 100 μM histamine, 2 μM ionomycin + 4 mM EGTA to determine R_{min} , followed by 5 μM ionomycin + 10 mM Ca²⁺ to determine R_{max} . (B, D, F, and H) Mitochondrial [Ca²⁺] calculated from the ratios before ionophore addition for the experiments presented in (A), (C), (E), and (G), respectively. The solid and dashed curves each represent a different cell.

One advantage of these improved mitochondrial cameleons is the ability to monitor Ca²⁺ dynamics within a single cell and thereby resolve subcellular heterogeneity. Figure 7 depicts data from a HeLa cell expressing 4mtD3cpv. Treatment with histamine results in dramatically different Ca²⁺ responses in two separate regions of the cell. Region A showed a rapid Ca²⁺ increase, followed by rapid decline, as can be seen from the time course and the individual pseudo color FRET images. In contrast, region B showed a rapid Ca²⁺ rise, followed by a much slower decline, with a single Ca²⁺ spike clearly visible on the decline. In an elegant study by Collins et al., it was previously demonstrated that mitochondria are morphologically and functionally heterogeneous, and that mitochondria in different regions (perinuclear versus peripheral) took up different amounts of Ca²⁺ [34]. Our work supports this finding and extends it to show that there is also heterogeneity in the decay of the Ca²⁺ response, which could have important consequences for downstream signaling processes, thus highlighting the need to examine mitochondrial Ca²⁺ in individual cells.

Significance

In the present work, we reengineered the binding interface between CaM and a 26 residue target peptide by computationally designing steric bumps in the peptide with complementary holes in CaM. The mutant CaM-peptide pairs led to the development of a new generation of cameleons that, in contrast to previous cameleons, were not perturbed by large excesses of CaM. This is an important step in the design of Ca²⁺ indicators that do not interfere with, nor are perturbed by, endogenous cellular proteins. Our new cameleons covered a 100-fold range in Ca²⁺ sensitivity ($K'_d = 0.6$ and 60 μM for D3cpv and D4cpv, respectively), making them useful in different subcellular locations (plasma membrane, mitochondria, microdomains, etc.). D3cpv will be particularly valuable to researchers who are monitoring small changes in Ca²⁺ above basal levels, as the K'_d for Ca²⁺ of D3cpv is poised directly between YC2.1 and YC3.3, but is no longer perturbed by excess CaM and has a ~5-fold increase in dynamic range. We demonstrated that D3cpv can be targeted to the plasma

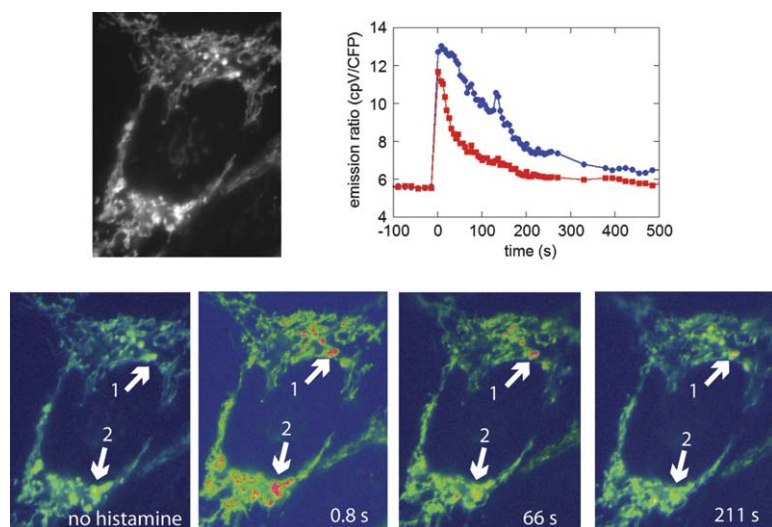


Figure 7. Spatial Heterogeneity in the Mitochondrial Ca^{2+} Response in an Individual Cell Expressing 4mtD3cpv

Upon treatment with 100 μM histamine, there is a rapid rise in mitochondrial Ca^{2+} in both regions 1 and 2. The Ca^{2+} in region 2 (red, squares) decreases much more rapidly than that in region 1 (blue, circles), which shows a slower decay and even shows a single Ca^{2+} spike upon decay. This can also be seen in the pseudo color FRET images in which region 1 maintains high Ca^{2+} (red) for much longer than region 2.

membrane of hippocampal neurons, where it was both sensitive to Ca^{2+} influx due to spontaneous activity and stimulated Ca^{2+} influx (KCl-induced depolarization, addition of exogenous glutamate, and electrical stimulation). Importantly, this redesigned cameleon remedied the problem of earlier cameleons that were unable to measure Ca^{2+} when targeted to the plasma membrane and enabled us to observe Ca^{2+} influx from single action potentials. D2cpv, D3cpv, and D4cpv were all targeted to the mitochondria by using tandem repeats of the CytC signal sequence. We have improved the localization and the sensitivity of these sensors and broadened the range of $[\text{Ca}^{2+}]$ they can measure; these changes led to a significant improvement in our ability to accurately and quantitatively image mitochondrial Ca^{2+} processes at the single-cell level.

Experimental Procedures

Abbreviations

The following abbreviations are used in this article: calmodulin, CaM; CFP, cyan fluorescent protein; cpV, circularly permuted Venus fluorescent protein; DIV, days *in vitro*; EGTA, ethylenedis(oxyethylene)triacetic acid; FRET, fluorescence resonance energy transfer; HEEDTA, (N-(2-hydroxyethyl)ethylenedinitrilo-N,N',N'-triacetic acid); K_d , apparent dissociation constant, or Ca^{2+} concentration at which the emission ratio is midway between the ratios at zero and saturating Ca^{2+} ; skMLCK or M13, skeletal muscle myosin light chain kinase; smMLCK, smooth muscle myosin light chain kinase; wt, wild-type; YFP, yellow fluorescent protein;

Computational Design

The crystal structure of CaM and smooth muscle myosin light chain kinase was used as the starting point for computationally designing the CaM-peptide interface (PDB code: 1CDL) [23]. The general computational design procedure has been described previously [25]. Briefly, the design algorithm modeled amino acid side chains as rotamers in an all-atom representation (heavy atoms plus polar hydrogens, where polar hydrogens were added as previously described [35]) with a fixed polypeptide backbone. The total energy of CaM-peptide complexes was optimized by using a Monte-Carlo simulated annealing procedure [36] and a free energy function as described previously [35–37]. Initially, a computational Ala scan was conducted to identify hot spots that contribute strongly to the binding energy, where the binding energy was calculated as described [24] and a hot spot was defined as $\Delta\Delta G \geq 1$ kcal/mol. Three residues

were selected for redesign (A13, I14, V11). The overall design strategy is outlined in the Results section.

Because the computational designs utilized the crystal structure of smMLCK with CaM, whereas the linker regions (sequences between the individual proteins) of the cameleon have been optimized for the CaM-skMLCK pair, we created a hybrid peptide in which the outskirts are skMLCK in origin and the central helix is smMLCK in origin. This peptide has the following sequence: KRRWQKTGHAVRAIGRLKKISSSGAL; residues from smMLCK are shown in bold.

Gene Construction

The mutant peptides and CaMs were generated by using a Quick-Change Multi kit (Stratagene). They were cloned between a slightly truncated (by 11 residues) enhanced cyan fluorescent protein [1] (ECFP) and either citrine (enhanced YFP with S65G, V68L, Q69K, S72A, and T203Y) [7] or circularly permuted 173 Venus [14] such that SphI and SacI sites were incorporated as linkers, thus generating a fusion of ECFP-CaM-GlyGly-peptide-GluLeu-citrine. Constructs that contain cp173Venus in place of citrine are denoted by cpv. The constructs were cloned between the BamHI/EcoRI sites in pRSETB (Invitrogen) or pBAD (Invitrogen) for protein purification. To generate a membrane-targeted cameleon, the myristoylation and palmitoylation sequence from lyn kinase (MGCIKSKRKDNLNDGDVDMKT) was added to the N terminus [31]. To target the constructs to the mitochondria, an extension of the strategy employed by Filipin et al. was employed [13]. Briefly, either 2, 4, 6, or 8 (2mt, 4mt, etc.) copies of the cytochrome c oxidase signal sequence (MSVLTPLLLRGLTGSARRLPVPRAKIHSLGDP) were added to the N terminus of ECFP. For expression in mammalian cells, constructs were cloned into pcDNA3 between HindIII and EcoRI.

In Vitro Characterization of the Cameleons

For protein purification, cameleons in either pRSETB or pBAD were transformed into either JM109 (Stratagene) or LMG194 (Invitrogen) and were grown overnight at 25°C. Constructs in pBAD/LMG194 were induced with 0.2% arabinose. Protein was extracted with Bacterial Protein Extraction Reagent (BPER, Pierce), in the presence of protease inhibitors (CompleteEDTA, Roche), and purified via an N-terminal 6×His tag by using Ni-NTA agarose (QIAGEN). Proteins were buffer exchanged into 10 mM MOPS, 100 mM NaCl (pH 7.4) by using Centricon-30 columns (Amicon). Absorbance measurements were conducted on a Cary 3E UV-Visible spectrometer. Fluorescence measurements were conducted on a Spex Fluorolog-3 Fluorometer (Horiba) at a cameleon concentration of 0.4 μM . Ca^{2+} /EGTA and Ca^{2+} /HEEDTA buffers were prepared as described previously [38, 39] and were used in Ca^{2+} titrations to achieve concentrations < 50 μM . All solutions > 50 μM were unbuffered. To test the effect of wt CaM on the sensors, CaM/pRSETB was transformed into JM109 and purified by 6×His affinity chromatography. The concentration of CaM was determined from the $\epsilon_{280} = 1500 \text{ M}^{-1} \text{ cm}^{-1}$ [40].

Cell Culture and Imaging

HeLa cells were plated on 10 cm plates or sterilized glass coverslips in 2 cm dishes and grown to 40%–80% confluency in DMEM (GIBCO-BRL) supplemented with low (1 g/l) glucose, 10% FBS, and 1% penicillin/streptomycin at 37°C and 6% CO₂. HeLa cells were transfected with FuGENE-6 transfection reagent (Roche Molecular Biochemicals) according to the manufacturer's instructions. Cells were imaged 2–3 days after transfection. Primary rat hippocampal neurons were cultured from 18-day-old rat embryos and day 0 postnatal rats and were maintained in Neurobasal media supplemented with B27 and 1% penicillin/streptomycin. Neurons were transfected by using a modified calcium phosphate protocol [41] on DIV (day-in-vitro) 10 and were imaged on DIV13. For imaging experiments, cells were rinsed twice and then maintained in Hanks' Balanced Salt Solution (HBSS) with 20 mM HEPES and 2 g/l D-glucose at pH 7.4. Comparable Ca²⁺-free solutions were prepared without Ca²⁺, but with all the other components.

For electrical stimulation experiments, 80V 0.7 ms pulses were delivered from a Grass stimulator through parallel platinum electrodes in a custom imaging chamber. Pulse timing and trace alignment was controlled by custom Visual Basic scripts. Cyan and yellow epifluorescence were simultaneously recorded at 30 frames/s and 40× magnification on an Olympus IX70 microscope with a Dual View beamsplitter (Optical Insights) coupled to a Hamamatsu EB-C7190 camera. A slow, stereotypical increase in cytosolic autofluorescence following trains of action potentials was corrected by subtraction. Between-trace photobleaching was negligible and was left uncorrected. The bath solution contained NaCl (140 mM), KCl (5 mM), glucose (33 mM), HEPES (25 mM), CaCl₂ (2 mM), and MgCl₂ (1.3 mM).

To calibrate the cameleons, R_{min} and R_{max} were obtained inside cells. R_{min} was obtained by treating the cells with 3 mM EGTA along with 2 μM ionomycin, and R_{max} was obtained by treating the cells with 5–8 μM ionomycin and 10 mM Ca²⁺. The in situ R_{min} and R_{max} values were used to convert live cell data to percent FRET (of max). Finally, the K'_d and R_{max} values obtained from in vitro data fits of D2cpv and D3cpv were used in the calibration. D2cpv required a two-site model to fit the in vitro data, where K'_{d1} (0.097), K'_{d2} (7.67), R_{max1} (65.9), R_{max2} (33.53), n₁ (1.34), and n₂ (0.77) were obtained from fitting the in vitro data with $R = \{R_{max1} [Ca^{2+}]^{n1} / (K'_{d1}{}^{n1} + [Ca^{2+}]^{n1})\} + \{R_{max2} [Ca^{2+}]^{n2} / (K'_{d2}{}^{n2} + [Ca^{2+}]^{n2})\}$. The D3cpv data were best fit by using a one-site Hill model in which the values K'_d (0.76), R_{max} (105.3), and n (0.74) were obtained by fitting the in vitro data with $R = R_{max} [Ca^{2+}]^n / (K'_{d}{}^n + [Ca^{2+}]^n)$. The data for D4cpv were best fit with a one site Hill model with K'_d (49.68), R_{max} (98.04), and n (1.35). The data for YC2 (in the 2mtYC2/pMito construct) were fit with the two-site Hill model with a K'_{d1} of 0.03, a K'_{d2} of 3.19, an R_{max1} of 50.6, and an R_{max2} of 45.03. For a one-site Hill model, the apparent dissociation constant (K'_d) is related to the true Ca²⁺ dissociation constant, K_d, by the equation [42] $K'_{d} = K_{d} (S_{f2}/S_{b2})^{1/n}$, where (S_{f2}/S_{b2}) is the ratio of emission intensities of the Ca²⁺-free cameleon to the Ca²⁺ bound cameleon, measured over the denominator wavelength passband, i.e., the FRET-excited YFP emission band. For cameleons incorporating cpVenus, (S_{f2}/S_{b2}) is about 0.47.

It should be noted that there are two factors that impact the R_{max} determination with ionomycin and Ca²⁺: (1) the ability of ionomycin/Ca²⁺ to saturate the probe in different cellular locations (cytosol versus mitochondria), and (2) a potential decrease in the overall FRET ratio due to acceptor (YFP) photobleaching under conditions of more intense illumination. These factors make calibrations of mitochondrial cameleons a bit more challenging than cytoplasmic cameleons. In particular, high levels of cytoplasmic Ca²⁺ can cause a change in mitochondrial morphology, which makes calibration of R_{max} more difficult. In spite of this complication, in the majority of experiments we were able to obtain R_{max} without gross morphological changes in mitochondria, and in these situations the overall ratio change was similar to that observed for the cytosolic cameleon sensor. However, we did observe more photobleaching of the mitochondrial cameleons because we often collected data at 100× rather than 40× and thus had to illuminate for longer (1000 ms versus 500 ms) to obtain images of comparable brightness. Additionally, we were subjecting the cells to significant illumination (data collection every 5 s in order to observe oscillations).

To obtain the percentage of fluorescence intensity of the different subcellular compartments compared to mitochondria, we calcu-

lated the average fluorescence intensity in different regions of the nucleus and mitochondria. For each value, we considered at least ten cells. The distribution of mistargeted distribution was calculated by counting the total number of the transfected cells and, among these, the number of cells with cytosolic staining.

Cells were imaged on a Zeiss Axiovert 200M microscope with a cooled CCD camera (Roper Scientific), controlled by METAFUOR 6.1 Software (Universal Imaging). Emission ratio imaging of the cameleon was accomplished by using a 436DF20 excitation filter, a 450 nm dichroic mirror, and two emission filters (475/40 for ECFP and 535/25 for citrine) controlled by a Lambda 10-2 filter changer (Sutter Instruments). Fluorescence images were background corrected. Exposure times were typically 600–1000 ms, and images were collected every 5–20 s. Data were collected either by using a 40× objective or, for the mitochondrially-targeted cameleon, a 2.5× OPTOVAR (i.e., effectively 100× objective magnification).

Supplemental Data

Supplemental Data including details of the computational design results and images of mitochondrial targeting are available at <http://www.chembiol.com/cgi/content/full/13/5/521/DC1/>.

Acknowledgments

We thank S.R. Adams, L. Gross, P. Steinbach, and Q. Xiong for assistance and advice. M.Z. Lin is acknowledged for help with culturing and transfection of primary rat hippocampal neurons. We thank A. Miyawaki for the gift of cp173Venus and Tullio Pozzan for the gift of 2mtYC2/pMito. This work was supported by a Ruth L. Kirschstein National Institutes of Health (NIH) postdoctoral fellowship (F32 GM067488-01 to A.E.P.), by a Human Frontier Science Program postdoctoral fellowship (LT00358/2000-M to T.K.), and by grants (NIH: NS27177 and Department of Energy: DE-FG-01-ER63276) to R.Y.T. and an NIH grant to D.B.

Received: December 15, 2005

Revised: March 16, 2006

Accepted: March 17, 2006

Published: May 29, 2006

References

- Miyawaki, A., Llopis, J., Heim, R., McCaffery, J.M., Adams, J.A., Ikura, M., and Tsien, R.Y. (1997). Fluorescent indicators for Ca²⁺ based on green fluorescent proteins and calmodulin. *Nature* 388, 882–887.
- Romoser, V.A., Hinkle, P.M., and Persechini, A. (1997). Detection in living cells of Ca²⁺-dependent changes in the fluorescence emission of an indicator composed of two green fluorescent protein variants linked by a calmodulin-binding sequence. *J. Biol. Chem.* 272, 13270–13274.
- Miyawaki, A., Griesbeck, O., Heim, R., and Tsien, R.Y. (1999). Dynamic and quantitative Ca²⁺ measurements using improved cameleons. *Proc. Natl. Acad. Sci. USA* 96, 2135–2140.
- Truong, K., Sawano, A., Mizuno, H., Hama, H., Tong, K.I., Mal, T.K., Miyawaki, A., and Ikura, M. (2001). FRET-based in vivo Ca²⁺ imaging by a new calmodulin-GFP type molecule. *Nat. Struct. Biol.* 8, 1069–1073.
- Heim, N., and Griesbeck, O. (2004). Genetically encoded indicators of cellular calcium dynamics based on troponin C and green fluorescent protein. *J. Biol. Chem.* 279, 14280–14286.
- Baird, G.S., Zacharias, D.A., and Tsien, R.Y. (1999). Circular permutation and receptor insertion within green fluorescent proteins. *Proc. Natl. Acad. Sci. USA* 96, 11241–11246.
- Griesbeck, O., Baird, G.S., Campbell, R.E., Zacharias, D.A., and Tsien, R.Y. (2001). Reducing the environmental sensitivity of yellow fluorescent protein. *J. Biol. Chem.* 276, 29188–29194.
- Nakai, J., Ohkura, M., and Imoto, K. (2001). A high signal-to-noise Ca²⁺ probe composed of a single green fluorescent protein. *Nat. Biotechnol.* 19, 137–141.
- Nagai, T., Sawano, A., Park, E.S., and Miyawaki, A. (2001). Circularly permuted green fluorescent proteins engineered to sense Ca²⁺. *Proc. Natl. Acad. Sci. USA* 98, 3197–3202.

10. Mank, M., Reiff, D.F., Heim, N., Friedrich, M.W., Borst, A., and Griesbeck, O.A. (2006). FRET-based calcium biosensor with fast signal kinetics and high fluorescence change. *Biophys. J.* **90**, 1790–1796.
11. Palmer, A.E., Jin, C., Reed, J.C., and Tsien, R.Y. (2004). Bcl-2-mediated alterations in endoplasmic reticulum Ca^{2+} analyzed with an improved genetically encoded fluorescent sensor. *Proc. Natl. Acad. Sci. USA* **101**, 17404–17409.
12. Filippin, L., Magalhaes, P.J., Benedetto, G.D., Colella, M., and Pozzan, T. (2003). Stable interactions between mitochondria and endoplasmic reticulum allow rapid accumulation of calcium in a subpopulation of mitochondria. *J. Biol. Chem.* **278**, 39224–39234.
13. Filippin, L., Abad, M.C., Gastaldello, S., Magalhaes, P.J., Sandona, D., and Pozzan, T. (2005). Improved strategies for the delivery of GFP-based Ca^{2+} sensors into the mitochondrial matrix. *Cell Calcium* **37**, 129–136.
14. Nagai, T., Yamada, S., Tominaga, T., Ichikawa, M., and Miyawaki, A. (2004). Expanded dynamic range of fluorescent indicators for Ca^{2+} by circularly permuted yellow fluorescent proteins. *Proc. Natl. Acad. Sci. USA* **101**, 10554–10559.
15. Kerr, R., Lev-Ram, V., Baird, G., Vincent, P., Tsien, R.Y., and Schafer, W.R. (2000). Optical imaging of calcium in neurons and pharyngeal muscle of *C. elegans*. *Neuron* **26**, 583–594.
16. Higashijima, S., Masino, M.A., Mandel, G., and Fetcho, J.R. (2003). Imaging neuronal activity during zebrafish behavior with a genetically encoded calcium indicator. *J. Neurophysiol.* **90**, 3986–3997.
17. Fiala, A., Spall, T., Diegelmann, S., Eisermann, B., Sachse, S., Devaud, J.-M., Buchner, E., and Galizia, C.G. (2002). Genetically expressed cameleon in *Drosophila melanogaster* is used to visualize olfactory information in projection neurons. *Curr. Biol.* **12**, 1877–1884.
18. Reiff, D.F., Thiel, P.R., and Schuster, C.M. (2002). Differential regulation of active zone density during long-term strengthening of *Drosophila* neuromuscular junctions. *J. Neurosci.* **22**, 9399–9409.
19. Reiff, D.F., Ihring, A., Guerrero, G., Isacoff, E.Y., Joesch, M., Nakai, J., and Borst, A. (2005). In vivo performance of genetically encoded indicators of neural activity in flies. *J. Neurosci.* **25**, 4766–4778.
20. Griesbeck, O. (2004). Fluorescent proteins as sensors for cellular functions. *Curr. Opin. Neurobiol.* **2004**, 636–641.
21. Mori, M.X., Erickson, M.G., and Yue, D.T. (2004). Functional stoichiometry and local enrichment of calmodulin interacting with Ca^{2+} channels. *Science* **304**, 432–435.
22. Hasan, M.T., Friedrich, R.W., Larkum, M.E., Euler, T., Both, M., Duebel, J., Waters, J., Bujard, H., Griesbeck, O., Tsien, R.Y., et al. (2004). Functional fluorescent Ca^{2+} indicator proteins in transgenic mice under TET control. *PLoS Sci.* **2**, e163.
23. Meador, W.E., Means, A.R., and Quijoco, F.A. (1992). Target enzyme recognition by calmodulin: 2.4 Å structure of a calmodulin-peptide complex. *Science* **257**, 1251–1254.
24. Kortemme, T., and Baker, D. (2002). A simple physical model for binding energy hot spots in protein-protein complexes. *Proc. Natl. Acad. Sci. USA* **99**, 14116–14121.
25. Kortemme, T., Joachimiak, L.A., Bullock, A.N., Schuler, A.D., Stoddard, B.L., and Baker, D. (2004). Computational redesign of protein-protein interaction specificity. *Nat. Struct. Mol. Biol.* **11**, 371–379.
26. Arnaudeau, S., Kelley, W.L., Walsh, J.V., Jr., and Demareux, N. (2001). Mitochondria recycle Ca^{2+} to the endoplasmic reticulum and prevent depletion of neighboring endoplasmic reticulum regions. *J. Biol. Chem.* **276**, 29430–29439.
27. Shifman, J.M., and Mayo, S.L. (2002). Modulating calmodulin binding specificity through computational protein design. *J. Mol. Biol.* **323**, 417–423.
28. Shifman, J.M., and Mayo, S.L. (2003). Exploring the origins of binding specificity through the computational redesign of calmodulin. *Proc. Natl. Acad. Sci. USA* **100**, 13274–13279.
29. Reina, J., Lacroix, E., Hobson, S.D., Fernandez-Ballester, G., Rybin, V., Serrano, L., and Gonzalez, C. (2002). Computer-aided design of a PDZ domain to recognize new target sequences. *Nat. Struct. Biol.* **9**, 621–627.
30. Havranek, J.J., and Harbury, P.B. (2003). Automated design of specificity in molecular recognition. *Nat. Struct. Biol.* **10**, 45–52.
31. Zacharias, D.A., Violin, J.D., Newton, A.C., and Tsien, R.Y. (2002). Partitioning of lipid-modified monomeric GFPs into membrane microdomains of live cells. *Science* **296**, 913–916.
32. Berridge, M.J., Lipp, P., and Bootman, M.D. (2000). The versatility and universality of calcium signalling. *Nat. Rev. Mol. Cell Biol.* **1**, 11–21.
33. Nagai, T., Ibata, K., Park, E.S., Kubota, M., Mikoshiba, K., and Miyawaki, A. (2002). A variant of yellow fluorescent protein with fast and efficient maturation for cell-biological applications. *Nat. Biotechnol.* **20**, 87–90.
34. Collins, T.J., Berridge, M.J., Lipp, P., and Bootman, M.D. (2002). Mitochondria are morphologically and functionally heterogeneous within cells. *EMBO J.* **21**, 1616–1627.
35. Kortemme, T., Morozov, A.V., and Baker, D. (2003). An orientation-dependent hydrogen bonding potential improves prediction of specificity and structure for proteins and protein-protein complexes. *J. Mol. Biol.* **326**, 1239–1259.
36. Kuhlman, B., and Baker, D. (2000). Native protein sequences are close to optimal for their structures. *Proc. Natl. Acad. Sci. USA* **97**, 10383–10388.
37. Lazaridis, T., and Karplus, M. (1999). Effective energy function for proteins in solution. *Proteins* **35**, 133–152.
38. Tsien, R.Y., and Pozzan, T. (1989). Measurement of cytosolic free Ca^{2+} with Quin2. *Methods Enzymol.* **172**, 230–263.
39. Tsien, R.Y., and Rink, T.J. (1983). Measurement of free Ca^{2+} in cytoplasm. In *Current Methods in Cellular Neurobiology*, J.L. Barber, ed. (New York: John Wiley & Sons), pp. 249–312.
40. Maune, J.F., Klee, C.B., and Beckingham, K. (1992). Ca^{2+} binding and conformational change in two series of point mutations to the individual Ca^{2+} -binding sites of calmodulin. *J. Biol. Chem.* **267**, 5286–5295.
41. Jiang, M., Deng, L., and Chen, G. (2004). High Ca^{2+} -phosphate transfection efficiency enables single neuron gene analysis. *Gene Ther.* **11**, 1303–1311.
42. Adams, S.R., Bacskai, B.J., Taylor, S.S., and Tsien, R.Y. (1993). Optical probes for cyclic AMP. In *Fluorescent Probes for Biological Activity of Living Cells - A Practical Guide*, W.T. Matson and G. Relf, eds. (New York: Academic Press), pp. 133–149.

Accession Numbers

Coordinates for D2cpv, D3cpv, D4cpv, lynD3cpv, and 4mtD3cpv have been deposited in GenBank with accession codes [DQ479425](#), [DQ479426](#), [DQ479427](#), [DQ479428](#), and [DQ479429](#), respectively.